Tasmanian devil CD28 and CTLA4 capture CD80 and CD86 from adjacent cells

Wong, C.; Darby, J.M.; Murphy, P.R.; Pinfold, T.L.; Lennard, P.R.; Woods, G.M.; ... ; Flies, A.S.

1 **Title**
2 Tasmanian devil CD28 and CTLA4 capture CD80 and CD86 from adjacent cells
3
4 **Running title**
5 Intercellular protein transfer of immune checkpoints in Tasmanian devils
6
7 **Article Type**
8 Short Communications
9

10 **Authors**
11 Candida Wong[a], Jocelyn M. Darby[a], Peter R. Murphy[a,b], Terry L. Pinfold[c], Patrick R.
12 Lennard[d], Gregory M Woods[a], A. Bruce Lyons[c], Andrew S. Flies[a]*
13
14 **Affiliations**
15 [a]Menzies Institute for Medical Research, College of Health and Medicine, University of
16 Tasmania, Hobart, TAS 7000, Australia
17 [b]University of Queensland Diamantina Institute, The University of Queensland, Translational
18 Research Institute, Woolloongabba, Queensland, Australia
19 [c]Tasmanian School of Medicine, College of Health and Medicine, University of Tasmania,
20 Hobart, TAS 7000, Australia
21 [d]The Roslin Institute and Royal School of Veterinary Studies, University of Edinburgh,
22 Easter Bush Campus, Midlothian, EH25 9RG, UK.
23
24 **Corresponding author**
25 Andrew S. Flies, PhD
26 Menzies Institute for Medical Research, College of Health and Medicine
27 University of Tasmania
28 Private Bag 23, Hobart TAS 7000
29 phone: +61 3 6226 4614; email: Andy.Flies@utas.edu.au
30
31
32

33 **Highlights**

34 • Key immune checkpoint receptor-ligand interactions are conserved in marsupials.

35 • Live cell-based assays show Tasmanian devil CD28 and CTLA4 can capture CD80

36 and CD86 *in trans* from adjacent cells.

37 • Mutation of the conserved CTLA4$_{MYPPPY}$ ligand binding motif to CTLA4$_{MYPPPA}$

38 reduces binding to CD80 and intercellular protein transfer.

39 • Removal of conserved CTLA4$_{YVKM}$ protein recycling binding motif in CTLA4 results

40 in bidirectional intercellular protein transfer between CTLA4 and CD80.

41 • Highly successful human immune checkpoint immunotherapies have the potential to

42 be translated for veterinary and conservation medicine.

43

44 **Abstract**

45 Immune checkpoint immunotherapy is a pillar of human oncology treatment with potential for

46 non-human species. The first checkpoint immunotherapy approved for human cancers targeted

47 the CTLA4 protein. CTLA4 can inhibit T cell activation by capturing and internalizing CD80

48 and CD86 from antigen presenting cells, a process called trans-endocytosis. Similarly, CD28

49 can capture CD80 and CD86 via trogocytosis and retain the captured ligands on the surface of

50 the CD28-expressing cells. The wild Tasmanian devil (*Sarcophilus harrisii*) population has

51 declined by 77% due to transmissible cancers that evade immune defenses despite genetic

52 mismatches between the host and tumours. We used a live cell-based assay to demonstrate that

53 devil CTLA4 and CD28 can capture CD80 and CD86. Mutation of evolutionarily conserved

54 motifs in CTLA4 altered functional interactions with CD80 and CD86 in accordance with

55 patterns observed in other species. These results suggest that checkpoint immunotherapies can

56 be translated to evolutionarily divergent species.

57

58   **Keywords**

59   immune checkpoint, wild immunology, transmissible cancer, trans-endocytosis, trogocytosis,

60   intercellular protein transfer

61   **Abbreviations**

62   intercellular protein transfer (IPT), devil facial tumour (DFT), interferon gamma (IFNγ), major

63   histocompatibility complex (MHC), Cytotoxic T-Lymphocyte Associated Protein 4 (CTLA4),

64   blue fluorescent protein (BFP)

65

66   **1. Introduction**

67   The initial USA Food and Drug Administration approval for an immune checkpoint

68   inhibitor was in 2011 when a monoclonal antibody targeting CTLA4 was approved for

69   metastatic melanoma (U.S. Food and Drug Administration, 2011). Since then, targeting

70   immune checkpoints has proved effective for many types of cancer, and a single monoclonal

71   antibody targeting the PD1 pathway is currently approved for 15 types of cancer (U.S. Food

72   and Drug Administration, 2020). Despite the massive potential for veterinary medicine and

73   One Health projects, functional comparative studies of immune checkpoints studies are limited,

74   and have focused primarily on domestic animals (Achleitner et al., 2011; Bernard et al., 2007;

75   Folkl et al., 2010; Hansen et al., 2009; Hartley et al., 2016; Ikebuchi et al., 2014, 2013, 2011;

76   Maekawa et al., 2014, 2017, 2016; Nemoto et al., 2018; Rebech et al., 2020; Tagawa et al.,

77   2016).

78   The Tasmanian devil (*Sarcophilus harrisii*) immune system has received attention in

79   recent years due to two transmissible cancers that have decimated the wild Tasmanian devil

80   population (Pearse and Swift, 2006; Pye et al., 2016). The original transmissible devil facial

81   tumor (DFT1) was first observed in 1996 and has since spread across most of the island state,

82   leading to an average 77% population decline in areas were the DFT1 is present (Lazenby et

83 al., 2018). In 2014, a second independent transmissible devil facial tumor (DFT2) was

84 discovered in southern Tasmania (Pye et al., 2016). DFT1 and DFT2 are lethal and the available

85 evidence suggests that both tumors have arisen from Schwann cells (Murchison et al., 2010;

86 Patchett et al., 2020). A primary means of immune evasion by DFT1 cells is downregulation

87 of MHC-I. However, MHC-I can be upregulated in response to IFNγ (Siddle et al., 2013). The

88 DFT2 cells examined to date generally express MHC-I (Caldwell et al., 2018). This suggests

89 that these transmissible cancers employ additional immune evasion mechanisms to induce

90 tolerance to tumor allografts and damage-associated molecular patterns.

91 We have shown that the immune checkpoint protein PDL1 binds to PD1 on DFT cells

92 and developed devil-specific monoclonal antibodies that can block this receptor-ligand

93 interaction (Flies et al., 2020a, 2016). Furthermore, exposure to IFNγ upregulates PDL1 on

94 DFT cells, matching the pattern observed in many human and mouse cancers. Comparative

95 sequence analysis of other key checkpoint proteins in devils showed that key regions in mouse

96 and human CD28 and CTLA4 proteins are conserved in devils (Flies et al., 2017). Additionally,

97 binding of CTLA4 to its ligands CD80 and CD86 has been confirmed using soluble

98 recombinant proteins (Flies et al., 2020a). However, functional analyses of cell surface protein

99 interactions and protein trafficking remain unexplored.

100 In humans and mice, CTLA4 can capture CD80 and CD86 from the surface of adjacent

101 cells via trans-endocytosis, which results in internalization and degradation of CD80 and CD86

102 in the capturing cell. CTLA4 is continuously recycled from the cell surface to endosomal

103 compartments, which allows a single CTLA4 protein to capture multiple ligands (Qureshi et

104 al., 2011; Robles et al., 2012). CTLA4-mediated depletion of CD80 and CD86 from antigen

105 presenting cells results in reduced T cell activation due to impaired CD28 costimulation

106 (Qureshi et al., 2011).

107   CD28 is known to capture CD80 and CD86 from the surface of adjacent cells, but the

108 captured ligands remain bound to CD28 on the surface of the capturing cell (Briggs, 2014;

109 Hwang et al., 2000; Qureshi et al., 2011). This process of trogocytosis has also been well-

110 documented for capture of MHC-I and MHC-II by T cells, NK cells, and basophils, and can

111 result in immune suppression due to depletion of MHC from target cells (Akkaya et al., 2019;

112 Chung et al., 2014; Daubeuf et al., 2006; Gu et al., 2012; Joly and Hudrisier, 2003; Lemaoult

113 et al., 2015; Nakayama et al., 2011).

114   We developed a panel of immune checkpoint proteins fused to fluorescent reporter

115 proteins and used coculture assays to monitor protein transfer using flow cytometry to

116 determine if intercellular protein transfer patterns evolutionarily conserved in Tasmanian

117 devils. This approach revealed that CTLA4 and CD28 can capture costimulatory ligands from

118 neighboring cells, and that key protein motifs for ligand binding and protein trafficking were

119 conserved in devils. The conserved functional interactions of these proteins across the 160

120 million years since the divergence of eutherian and metatherian mammals (Luo et al., 2011)

121 suggests strong stabilising selection and that there is potential to replicate successful human

122 immunotherapies in devils and other species.

123 **2. Materials and methods**

124 ***2.1 Design of expression vectors***

125   Complete methodological details with step-by-step instructions for (a) *in silico*

126 characterization of protein structure, (b) design and (c) assembly of expression vectors, and (d)

127 transfection of mammalian cells has been previously published (Flies et al., 2020a, Flies et al.,

128 under review at Bio-protocol).

129   Open reading frames for the devil genes of interest (CD28, CTLA4, CD80, and CD86)

130 were retrieved from Genbank and Ensembl databases (Table S1). *In silico* analysis of the

131 protein coding sequences for genes-of-interest in this study were performed in a previous study

132 (Flies et al., 2017). The expression vector design included the full-length open reading frames

133 for gene-of-interest fused to a tobacco etch virus cleavage tag, a linker peptide, a 6x-Histidine

134 purification tag, and monomeric fluorescent reporter protein. The direct fusion of the protein-

135 of-interest to a fluorescent reporter protein allow for protein tracking in live cells (Flies et al.,

136 2020a). The vectors contain an all-in-one transfection system that includes antibiotic resistance

137 and genes-of-interest within a Sleeping Beauty transposon cassette (Kowarz et al., 2015), and

138 the Sleeping Beauty transposase outside of the transposon cassette (Mátés et al., 2009).

139 CTLA4, CD28, CD80, and CD86 were fused to mCitrine (Addgene # 135923), mOrange

140 (Addgene # 135928), mTagBFP (Addgene # 135924), and mNeptune2 (Addgene # 135927),

141 respectively.

142 **_2.2 Restriction digest of expression vectors_**

143 2 µg of base expression vectors were digested using NotI-HF (NEB # R3189S) and

144 SmaI (NEB # R0141S) overnight at room temperature. Antarctic phosphatase (NEB #

145 M0289S) was then added to the vector digests and incubated for 60 minutes at 37°C, then for

146 a further 2 minutes at 80°C to inactivate the enzymes. The reactions were then run at 100V in

147 a 1% agarose gel and the digest vectors were excised and purified using a NucleoSpin® Gel

148 and PCR Clean-up Kit (Macherey-Nagel, USA) according to instructions set by the

149 manufacturer. DNA concentrations were measured and analysed using a NanoDrop™ 1000

150 Spectrophotometer (NanoDrop Technologies, USA).

151 **_2.3 Overlap extension PCR to create vector inserts_**

152 Overlap extension PCR was used to extend open reading frames and remove the stop

153 codon from the genes of interest to allow for Gibson assembly of plasmids pCW1, pCW2,

154 pCW3, and pCW5 (Gibson et al., 2009). Primers and reaction conditions are available in Table

155 S2. PCR amplicons were isolated using gel electrophoresis run at 100 V for 30 minutes in a

156 1% agarose gel. DNA was purified and quantified as described above. CTLA4 mutants with a

157   truncated C-terminus (pCW9; CTLA4$_{truncated}$; amino acids 211-223 deleted) or the YVKM

158   protein trafficking motif deleted (pCW8; CTLA4$_{del}$; amino acids 201-223 deleted) were

159   developed as previously described by Qureshi et al. (2012) with minor modifications. pCW8

160   and pCW9 were made by amplifying with a reverse primer that amplified the DNA upstream

161   of the deleted region and extension that overlapped the expression vector (Table S2). The

162   CTLA4 expression vector (pCW10) with an altered binding motif was produced by substituting

163   an alanine for the for the second tyrosine in the MYPPPY ligand binding motif (Y139A) to

164   create the CTLA4$_{MYPPPA}$ mutant (Morton et al., 1996). The mutation was coded into new

165   forward and reverse primers (Table S2), and were used to amplify and extend one fragment

166   upstream of the mutation, and one fragment downstream of the mutation. The two fragments

167   were purified, combined in a PCR reaction, and re-amplified using the forward from the 5'

168   fragment and the reverse primer from the 3' fragment to form one large fragment. This fragment

169   was purified and assembled using NEBuilder as described above.

170   *2.4 Assembly and transformation of expression vectors*

171   The DNA for the gene-of-interest with overlap extensions were ligated into the

172   digested vectors using NEBuilder® HiFi DNA Assembly Cloning Kit (NEB # E5520S) by

173   incubating at 50 °C for one hour according to the manufacturer's instructions. A negative

174   control was established by transforming DH5α with the linearised vector. A positive control

175   on the other hand was established by transforming DH5α bacteria with NEBuilder® Positive

176   Control (New England Biolabs, USA). After transformation, the bacteria were grown overnight

177   at 37°C on Luria Broth Agar plates added with 100 μg/mL of ampicillin.

178   Colony PCR was used to identify colonies with the predicted insert size. 10 μL of

179   OneTaq Quick-Load 2X Master Mix (NEB # M0486L) was used for all colony PCR. 7 μL of

180   deionized-distilled water was added to the mix, and then 1 μL of forward (pSB_EF1a.FOR:

181   GCCTCAGACAGTGGTTCAAAG)   and   reverse   (pSB_BGH.REV:

182   AGGCACAGTCGAGGCTGAT) primers at 10 μM concentration were diluted into the mix. 4

183   to 6 bacterial colonies were picked using sterile pipette tips and transferred to separate tubes

184   containing 10 μL of PBS for assessing. 1 uL of bacteria in PBS was then transferred to the PCR

185   tube to achieve a final volume of 20 μL and primer concentration of 0.5 μM. The mix was then

186   denatured at 94 °C for 5 minutes, and then subjected to 30 cycles of denaturation at 94 °C for

187   15 seconds, annealing at 58 °C for 15 seconds, and extension at 68 °C for 105 seconds, before

188   a final extension step at 72 °C for 3 minutes. 10 μL of the reaction was then added directly to

189   a 1% agarose gel and run at 100 V for 25-35 minutes. DNA bands were imaged under UV light

190   using Gel Doc™ XR+ Gel Documentation System (Bio-Rad, USA).

191   *2.5 Purification and sequencing of expression vectors*

192   Colonies that yielded amplicons that matched the predicted amplicon size were cultured

193   overnight for plasmid amplification. 9 μl of bacteria in PBS was added to 5 mL of Luria Broth

194   with 100 μg/ml of ampicillin. The bacterial cultures were incubated at 37°C and 200 rpm

195   overnight. The plasmids were isolated from bacterial culture using PureLink™ Quick Plasmid

196   Miniprep Kit (Invitrogen, USA) or NucleoSpin® Plasmid EasyPure Miniprep Kit (Macherey-

197   Nagel, USA) according to the manufacturers' instructions. Concentrations of purified plasmids

198   were quantified using a NanoDrop™ 1000 Spectrophotometer (NanoDrop Technologies,

199   USA). The plasmids were stored at -20°C. The plasmids were sequenced using a BigDye™

200   Terminator v3.1 Cycle Sequencing Kit (Applied Biosystems, USA).   The BigDye™

201   Terminator was removed using Agencourt® CleanSEQ® (Beckman Coulter, USA) according

202   to the protocols set by the manufacturer before loading samples to the Applied Biosystems®

203   3500xL Genetic Analyzer (Applied Biosystems, USA) for sequencing using a fluorescence-

204   based capillary electrophoresis analytical technique.

205   *2.6 Transfection of Chinese Hamster Ovary (CHO) cells*

206   CHO-K1 (ATCC CCL-61) cells were cultured in cRF10 (complete RPMI media

207   supplemented with 10% fetal bovine serum) in 75 cm^2 culture flasks (Corning, USA) at 37°C

208   in a humidified atmosphere with 5% CO_2. CHO cells were transfected using a modified

209   polyethylenimine-based (PEI) method. 300,000 cells/well were seeded into 6-well plates and

210   were grown overnight at 37°C with 5% CO_2. 2 µg of plasmid DNA and 6 µg of PEI were

211   diluted separately to 100 µL of PBS in separate microfuge tubes. The solution from the DNA

212   tube was then added to PEI tubes and mixed by gentle pipetting. Tubes with a total volume of

213   200 µl of reagents were incubated for 15 to 20 minutes at room temperature. While the

214   DNA:PEI solution was incubating the media on the target CHO cells in 6-well plates was

215   replaced with fresh cRF10. The transfection was accomplished by adding the entire contents

216   of DNA:PEI solution (200 µL) dropwise to the cells. Cells were then incubated with

217   transfection reagents overnight and examined for fluorescence on the Leica-DM IRB

218   fluorescence microscope (Leica, Germany). After fluorescence was detected indicating that

219   transfection was successful, the media was removed and replaced with cRF10 containing 1

220   mg/mL of hygromycin B solution from *Streptomyces hydroscopicus* (Invitrogen, USA). Media

221   was refreshed as needed until drug selection was complete and all cells were fluorescent. The

222   cells were then cultured in cRF10 with a maintenance dose of 0.2 mg/mL of hygromycin B.

223   *2.7 Intercellular protein transfer coculture assay*

224   The coculture assay to assess intercellular protein transfer was modified from Briggs

225   (2014). The lysosomal inhibitor chloroquine was used to block degradation of captured proteins

226   that were endocytosed (Qureshi et al., 2011). Chloroquine was diluted to 100 µM in cRF5

227   (complete RPMI with 5% fetal bovine serum) and 100 µL were added into appropriate wells

228   in a 96-well round bottom plate (Costar, USA). The plate was incubated at 37°C with 5% CO_2

229   until cell lines were ready to be cocultured. Stably-transfected CHO cells were harvested,

230   washed, and resuspended to 5 x 10^5 cells/mL in cRF5. 50 µL (25,000 cells) of cell line A (e.g.

231   CD28) and cell line B (e.g. CD80) were aliquoted into appropriate wells to achieve a 1:1 ratio

232   and a total of 50,000 cells/well. The final volume was 200 µL/well with a final chloroquine

233   concentration of 50 µM. The plates were then incubated at 37°C with 5% CO_2 for either 3 hours

234   or 20 hours.

235   **2.8 Flow cytometry**

236   The coculture assay plates were centrifuged at 500g for 3 minutes at 4°C. The 96-well

237   plate was then inverted, and the media was discarded by briskly dumping the media out. 100

238   µL of PBS was added into appropriate wells to wash cells and the plate was spun again at 500g

239   for 3 minutes at 4°C. After removing media, 100 µL of Trypsin-EDTA was added into each

240   well and incubated at 37°C with 5% CO_2 for 5 to 10 minutes or until cells were dislodged from

241   the bottom of the well. 150 µL of cRF10 was then added to each well and the cells were

242   resuspended by pipetting. The plate was then centrifuged at 500g for 3 minutes at 4°C and

243   media was discarded. 200 µL of flow cytometry buffer was added into each well. Following

244   this, the plate was spun again at 500g for 3 minutes at 4°C. Media was discarded and cells were

245   resuspended in 250 µL of flow cytometry fixation buffer (Flies et al., 2020a). The coculture

246   plate was placed on a rocking platform and incubated at room temperature and protected from

247   light for at least 20 minutes. The incubated plate was subsequently spun at 500g for 3 minutes

248   at 4°C and the media was discarded (Flies et al., 2020a). Cells in each well were resuspended

249   in 250 µl of flow cytometry buffer, wrapped in foil, and stored at 4°C for at least 2 hours before

250   flow cytometric analysis.

251   **2.9 Data Processing and Gating Strategy for Flow Cytometry Analysis**

252   Flow cytometry data was analysed using the FCS Express 6 Flow Cytometry Software

253   version 6 (De Novo Software). CHO cells were primarily gated by forward scatter height (FSC-

254   H) and side scatter height (SSC-H) to exclude cell debris, and then sub-gated for singlets using

255   FSC-A (area) and FSC-H. CHO cells that did not express a fluorescent protein or expressed a

256   single fluorescent protein were used as controls for setting voltages and compensation. A

257   minimum of 10,000 cells was acquired from each experimental sample, and all cell

258   combinations were done with n=3 technical replicates.

259   Intercellular protein transfer was identified according to the schematic in **Fig. 1A**. The

260   upper left quadrant (UL) and lower right quadrant (LR) indicate cells that have only a single

261   color of fluorescent protein (**Fig. 1A**). The upper right quadrant (UR) indicates cells that are

262   positive for two colors, indicating the intercellular transfer of a fluorescent protein occurred

263   (Briggs, 2014). Additionally, a shift in both cell lines to the UR quadrant indicates a

264   bidirectional protein exchange, whereas a shift from one of the cell lines to the UR quadrant

265   indicates a one-way protein transfer (**Fig. 1A**).

266   **2.10 Analysis of CTLA4 binding and protein trafficking motifs across species**

267   CTLA4 protein sequences were obtained from the National Center for Biotechnology

268   Information   (NCBI)   (https://www.ncbi.nlm.nih.gov/gene/1493/ortholog/).   Descriptive

269   information for CTLA4 for each class (*Amphibia, Reptilia, Aves, Mammalia*) were exported

270   separately from NCBI as tabular data (e.g. comma separated values spreadsheet). The files

271   were manually updated to include a new column containing the class (e.g. *Aves*). The

272   descriptive spreadsheets were then combined to create a spreadsheet with descriptive

273   information for all species. The RefSeq protein sequences were exported from NCBI as a

274   FASTA file. FASTA sequences were imported into CLC Main Workbench (CLC, 2020), and

275   the "Show Table" tab was used to determine the length of each CTLA4 protein sequence. This

276   table was copied and saved as a .CSV file for subsequent merging with other spreadsheets. The

277   "Motif Search" function in CLC was then used to identify and annotate all sequences containing

278   a greater than 90% match to the $CTLA4_{MYPPPY}$ and $CTLA4_{YVKM}$ motifs. A new .CSV file was

279   created for the $CTLA4_{MYPPPY}$ and the $CTLA4_{YVKM}$ matches. The four .CSV files were then

280   merged in R version 3.6.1 using the "merge" function (R Core Team, 2019). The script is

281   available with the supplementary material (r_CTLA4_merge_master.R) and the merged data

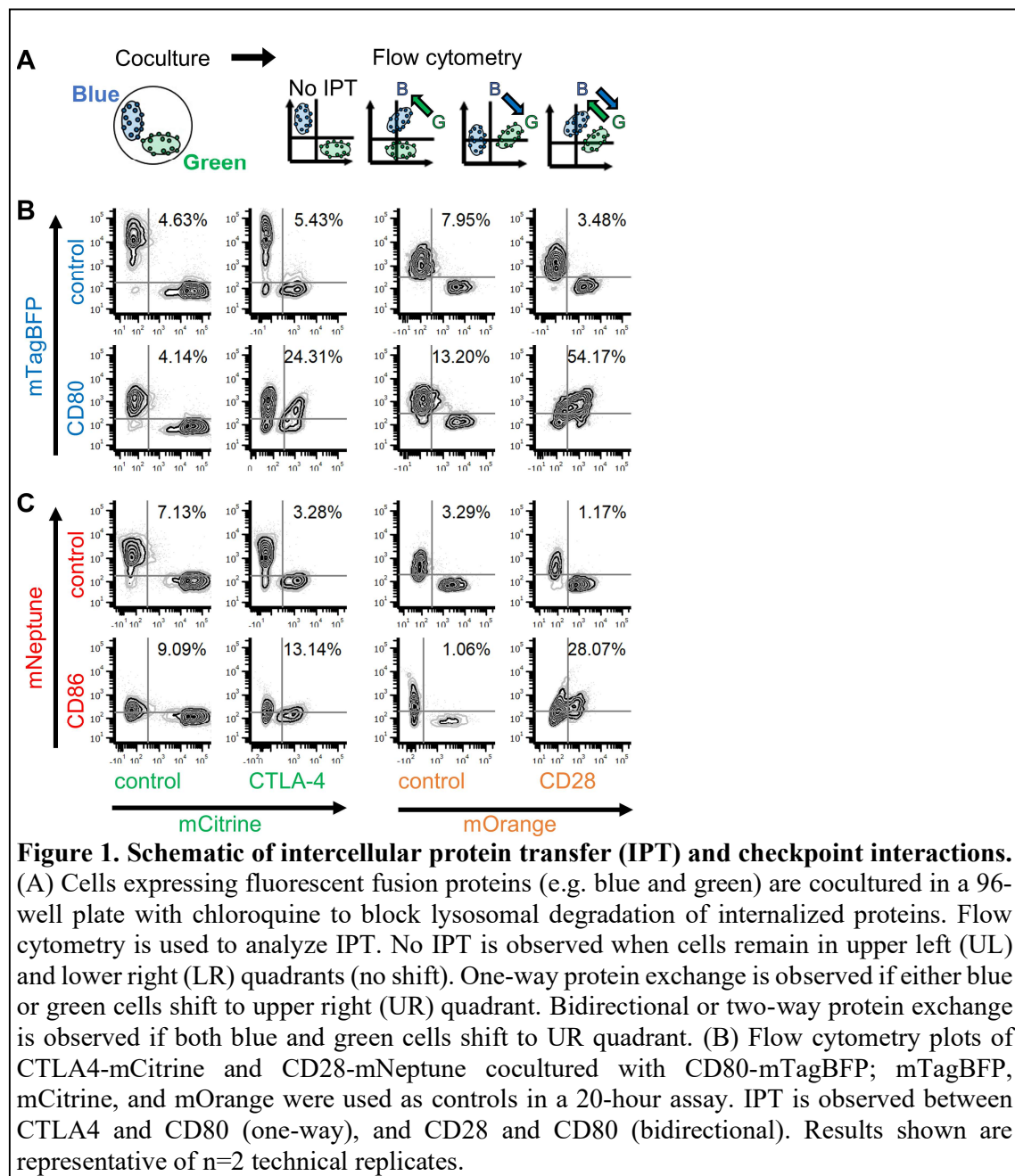282   are available in Table S3.

3. Results and Discussion

284   CHO cells expressing either unfused mCitrine or mTagBFP controls resulted in the

285   cells remaining primarily positive for only a single color after coculture (**Fig. 1B**). Likewise,

286   cells remained mostly single color positive after coculture of CTLA4-mCitrine with mTagBFP

287   control or mCitrine control with CD80-mTagBFP (**Fig. 1B**). However, coculture of CTLA4-

288   mCitrine with CD80-mTagBFP for 20 hours resulted in 24% of the cells in the upper right

289   quadrant. CTLA4 cells shifted from the lower right quadrant to the upper right quadrant

290   indicating positive receptor-ligand binding and protein transfer from CD80-mTagBFP to

291   CTLA4-mCitrine (**Fig. 1B**). The coculture between cells transfected with CD28-mOrange and

292   CD80-mTagBFP suggests that bidirectional protein transfer occurred as both single color

293   populations shifted, with 54% of the cells were in the upper right quadrant after coculture.

294   CTLA4 also captured CD86, whereas transfer of CD28 and CD86 again appeared to be

295   bidirectional (**Fig. 1C**). The interaction of CTLA4 and CD28 with CD80 appears stronger than

296   with CD86, but this could be an artefact of the suboptimal excitation of the mNeptune

297   fluorescent protein; mNeptune has peak excitation at 600 nm, but our available flow cytometer

298   had a 633 nm laser.

299   To assess the role of key functional motifs in CTLA4 we developed three CTLA4

300   mutants (**Fig. 2A**). Here, we used 3-hour and 20-hour coculture assays to document IPT over

301   time, and also to minimise potential side effects of extended cell culture with chloroquine. The

302   results show a one-way IPT from CD80-mTagBFP to CTLA4-mCitrine in 3-hour (17%) and

303   20-hour (46%) assays (**Fig. 2B**). The devil mutant truncated CTLA4$_{truncated}$-mCitrine (**Fig. 2B**)

304   also showed one-way protein exchange in both 3-hour (16%) and 20-hour (44%) assays with

305   CD80 (**Fig. 2B**). The YVKM motif in the cytoplasmic domain of CTLA4 is important for
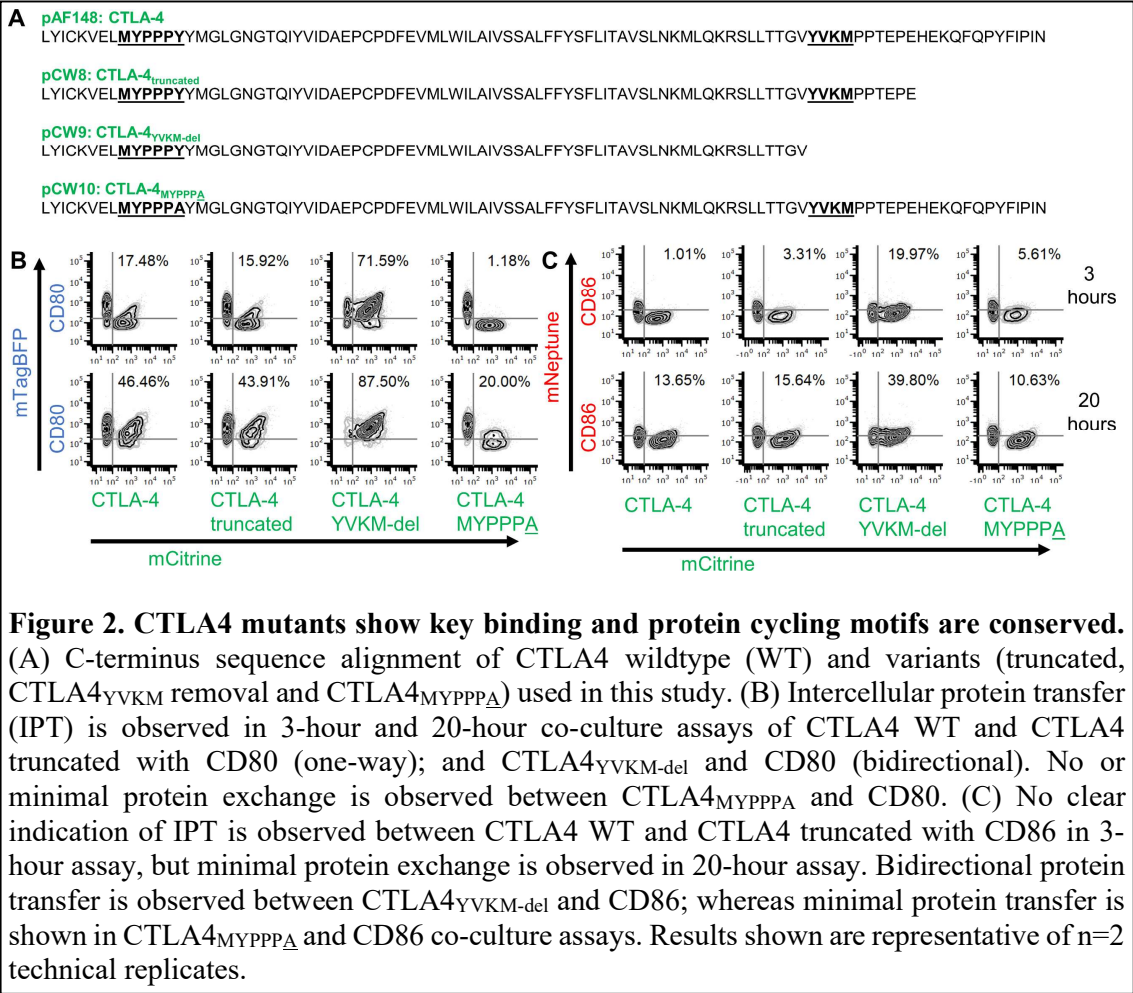
306 protein recycling, so we hypothesized that CTLA4-CD80 binding would remain intact in a

307 CTLA4 mutant with the YVKM motif removed, but that CTLA4 would have reduced capacity

308 to trans-endocytose CD80 and CD86. As expected, deletion of the YVKM dramatically

309 resulted in a pattern more closely resembling the interaction of CD28-CD80 than the CD80

310 with the other CTLA4 variants (**Fig. 2B**). The CTLA4 and CD86 interaction was also changed

311 in the CTLA4$_{YVKM-del}$ mutant, with the CTLA4 and CD86 populations merging towards a single

312 population after coculture.

313   In all species studied to date, the MYPPPY motif is required for ligand binding, so we

314 hypothesized that IPT would be reduced in cocultures using the CTLA4$_{MYPPPA}$ mutant

315 compared to other CTLA4 variants (**Fig. 2A**). Coculture of CD80 with mutant CTLA4$_{MYPPPA}$

316 showed minimal or no protein transfer (3-hours: 1%; 20-hours: 20%) (**Fig. 2B**), suggesting that

317 the MYPPPY motif is critical for CTLA4-CD80 binding interactions in Tasmanian devils. The

318 coculture of devil CTLA4 WT and CTLA4 mutants with CD86 ligand did not reveal a clear

319 indication of intercellular protein exchange in the 3-hour assay even though the flow cytometry

320 results showed a slight shift of CTLA4 (WT and mutants) to the UR quadrant (**Fig. 2C**).

321 However, 20-hour coculture assays revealed a one-way protein exchange from CD86-

322 mNeptune to CTLA4 WT-mCitrine (14%) and CTLA4 truncated-mCitrine (16%) (Fig. 2C).

323 Additionally, cells expressing mutant CTLA4$_{YVKM-del}$ cocultured with CD86 showed

324 bidirectional protein transfer between both cell lines in both 3-hour (20%) and 20-hour (40%)

325 assays (Fig. 2C). Lastly, CD86-mNeptune cocultured with mutant CTLA4 MYPPP<u>A</u> exhibited

326 minimal protein exchange in 20-hour assay (11%) (**Fig. 2C**).

Figure 1. Schematic of intercellular protein transfer (IPT) and checkpoint interactions. (A) Cells expressing fluorescent fusion proteins (e.g. blue and green) are cocultured in a 96-well plate with chloroquine to block lysosomal degradation of internalized proteins. Flow cytometry is used to analyze IPT. No IPT is observed when cells remain in upper left (UL) and lower right (LR) quadrants (no shift). One-way protein exchange is observed if either blue or green cells shift to upper right (UR) quadrant. Bidirectional or two-way protein exchange is observed if both blue and green cells shift to UR quadrant. (B) Flow cytometry plots of CTLA4-mCitrine and CD28-mNeptune cocultured with CD80-mTagBFP; mTagBFP, mCitrine, and mOrange were used as controls in a 20-hour assay. IPT is observed between CTLA4 and CD80 (one-way), and CD28 and CD80 (bidirectional). Results shown are representative of n=2 technical replicates.

327

328

A pAF148: CTLA-4
LYICKVEL**MYPPPY**YMGLGNGTQIYVIDAEPCPDFEVMLWILAIVSSALFFYSFLITAVSLNKMLQKRSLLTTGV**YVKM**PPTEPEHEKQFQPYFIPIN

pCW8: CTLA-4$_{truncated}$
LYICKVEL**MYPPPY**YMGLGNGTQIYVIDAEPCPDFEVMLWILAIVSSALFFYSFLITAVSLNKMLQKRSLLTTGV**YVKM**PPTEPE

pCW9: CTLA-4$_{YVKM-del}$
LYICKVEL**MYPPPY**YMGLGNGTQIYVIDAEPCPDFEVMLWILAIVSSALFFYSFLITAVSLNKMLQKRSLLTTGV

pCW10: CTLA-4$_{MYPPPA}$
LYICKVEL**MYPPPA**YMGLGNGTQIYVIDAEPCPDFEVMLWILAIVSSALFFYSFLITAVSLNKMLQKRSLLTTGV**YVKM**PPTEPEHEKQFQPYFIPIN

Figure 2. CTLA4 mutants show key binding and protein cycling motifs are conserved. (A) C-terminus sequence alignment of CTLA4 wildtype (WT) and variants (truncated, CTLA4$_{YVKM}$ removal and CTLA4$_{MYPPPA}$) used in this study. (B) Intercellular protein transfer (IPT) is observed in 3-hour and 20-hour co-culture assays of CTLA4 WT and CTLA4 truncated with CD80 (one-way); and CTLA4$_{YVKM-del}$ and CD80 (bidirectional). No or minimal protein exchange is observed between CTLA4$_{MYPPPA}$ and CD80. (C) No clear indication of IPT is observed between CTLA4 WT and CTLA4 truncated with CD86 in 3-hour assay, but minimal protein exchange is observed in 20-hour assay. Bidirectional protein transfer is observed between CTLA4$_{YVKM-del}$ and CD86; whereas minimal protein transfer is shown in CTLA4$_{MYPPPA}$ and CD86 co-culture assays. Results shown are representative of n=2 technical replicates.

329

330   CTLA4 orthologues for 233 species are listed in the GenBank data base (accessed 8-

331 May-2020; Table S3) (Benson et al., 2012). The CTLA4$_{MYPPPY}$ and CTLA4$_{YVKM}$ motifs are

332 conserved in 137 and 138, respectively, of the 140 mammalian species. The CTLA4$_{MYPPPY}$

333 motif is conserved in all 76 bird species in GenBank with CTLA4 orthologues, and the

334 CTLA4$_{MYPPPY}$ motif is conserved in 75 bird species. Only 3 reptiles have the CTLA4$_{MYPPPY}$

335 motif and 4 have the CTLA4$_{YVKM}$ motif. All three amphibians have the CTLA4$_{MYPPPY}$ motif,

336 but none have the CTLA4$_{YVKM}$ motif. The coculture assays described here is amenable for

337 functional testing of cell surface interactions in any of the above species, without the need to

338 purify recombinant proteins. However, primary cells for each species or amphibian, reptilian,

339 avian cell lines should be used instead of mammalian cell lines.

340   In summary, our results and analyses suggest that strong stabilizing selection has

341   operated to maintain the function of these key immune checkpoint genes. This opens the door

342   to immunotherapies that target these proteins for most mammalian species, and potentially for

343   most bird species and some reptiles and amphibians. Although we have focused on marsupials

344   in this manuscript, we believe that these methods can potentially be applied to the study of

345   receptor-ligand interactions in invertebrates. We have published step-by-step protocols to

346   facilitate comparative immunology studies in other non-model species (Flies et al., 2020b).

347   **Supplementary materials**

348   **Table S1. Summary of genes and plasmids**

349   **Table S2. Primer sequences for plasmid assembly**

350   **Table S3. Primer sequences for Sanger sequencing**

351

362

363

364

Author contributions

ASF and CW designed the study; ASF, CW, JMD, PRL, PRM, and TLP developed the

technology; CW performed the experiments; ASF and CW created the figures; ASF, CW,

TPL, ABL, and GMW analyzed the data; CW, ASF, and GMW wrote the manuscript and all

authors edited the manuscript.

Availability of data and materials

Data is available upon request, and will be made freely available in the University of

Tasmania Research Data Portal (https://rdp.utas.edu.au) following peer-reviewed publication.

Conflict of interest

The authors have no conflict of interest to report.

References

Achleitner, A., Clark, M.E., Bienzle, D., 2011. T-regulatory cells infected with feline

    immunodeficiency virus up-regulate programmed death-1 (PD-1). Vet. Immunol.

    Immunopathol. 143, 307–313. https://doi.org/10.1016/j.vetimm.2011.06.009

Akkaya, B., Oya, Y., Akkaya, M., Al Souz, J., Holstein, A.H., Kamenyeva, O., Kabat, J.,

    Matsumura, R., Dorward, D.W., Glass, D.D., Shevach, E.M., 2019. Regulatory T cells

    mediate specific suppression by depleting peptide–MHC class II from dendritic cells.

    Nat. Immunol. 20, 218–231. https://doi.org/10.1038/s41590-018-0280-2

Benson, D.A., Cavanaugh, M., Clark, K., Karsch-Mizrachi, I., Lipman, D.J., Ostell, J.,

    Sayers, E.W., 2012. GenBank. Nucleic Acids Res. 41, D36–D42.

    https://doi.org/10.1093/nar/gks1195

Bernard, D., Hansen, J.D., Du Pasquier, L., Lefranc, M.P., Benmansour, A., Boudinot, P.,

390   2007. Costimulatory receptors in jawed vertebrates: Conserved CD28, odd CTLA4 and

391   multiple BTLAs. Dev. Comp. Immunol. 31, 255–271.

392   https://doi.org/10.1016/j.dci.2006.06.003

393   Briggs, Z.L., 2014. CD28 costimulation in T cells: requirements, outcomes and regulation.

394   PhD Thesis.

395   Caldwell, A., Coleby, R., Tovar, C., Stammnitz, M.R., Mi Kwon, Y., Owen, R.S., Tringides,

396   M., Murchison, E.P., Skjødt, K., Thomas, G.J., Kaufman, J., Elliott, T., Woods, G.M.,

397   Siddle, H.V.T., 2018. The newly-arisen devil facial tumour disease 2 (DFT2) reveals a

398   mechanism for the emergence of a contagious cancer. Elife 7.

399   https://doi.org/10.7554/eLife.35314

400   Chung, B., Tor, John, Beilhack, G., Andersen, E., Brian, Jeffrey, Peter, 2014. Antigen-

401   Specific Inhibition of High-Avidity T Cell Target Lysis by Low-Avidity T Cells via

402   Trogocytosis 8, 871–882. https://doi.org/10.1016/j.celrep.2014.06.052

403   CLC, 2020. CLC Main Workbench.

404   Daubeuf, S., Puaux, A.-L., Joly, E., Hudrisier, D., 2006. A simple trogocytosis-based method

405   to detect, quantify, characterize and purify antigen-specific live lymphocytes by flow

406   cytometry, via their capture of membrane fragments from antigen-presenting cells. Nat.

407   Protoc. 1, 2536.

408   Flies, A.S., Blackburn, N.B., Lyons, A.B., Hayball, J.D., Woods, G.M., 2017. Comparative

409   analysis of immune checkpoint molecules and their potential role in the transmissible

410   Tasmanian devil facial tumor disease. Front. Immunol. 8, 513.

411   https://doi.org/10.3389/fimmu.2017.00513

412   Flies, A.S., Darby, J.M., Lennard, P.R., Murphy, P.R., Ong, C.E.B., Pinfold, T.L., De Luca,

413   A., Lyons, A.B., Woods, G.M., Patchett, A.L., 2020a. A novel system to map protein

414   interactions reveals evolutionarily conserved immune evasion pathways on transmissible

415   cancers. Sci. Adv. 6, eaba5031. https://doi.org/10.1126/sciadv.aba5031

416   Flies, A.S., Darby, J.M., Murphy, P.R., Pinfold, T.L., Patchett, A.L., Lennard, P.R., 2020b.

417   Fluorescent Adaptable Simple Theranostic (FAST) Proteins. Bio-protocol.

418   Flies, A.S., Lyons, A.B., Corcoran, L.M., Papenfuss, A.T., Murphy, J.M., Knowles, G.W.,

419   Woods, G.M., Hayball, J.D., 2016. PD-L1 Is Not Constitutively Expressed on

420   Tasmanian Devil Facial Tumor Cells but Is Strongly Upregulated in Response to IFN-γ

421   and Can Be Expressed in the Tumor Microenvironment. Front. Immunol. 7, 581.

422   https://doi.org/10.3389/fimmu.2016.00581

423   Folkl, A., Wen, X., Kuczynski, E., Clark, M.E., Bienzle, D., 2010. Feline programmed death

424   and its ligand: Characterization and changes with feline immunodeficiency virus

425   infection. Vet. Immunol. Immunopathol. 134, 107–114.

426   https://doi.org/10.1016/j.vetimm.2009.10.019

427   Gibson, D.G., Young, L., Chuang, R.-Y., Venter, J.C., Hutchison, C. a, Smith, H.O., Iii,

428   C.A.H., America, N., 2009. Enzymatic assembly of DNA molecules up to several

429   hundred kilobases. Nat. Methods 6, 343–5. https://doi.org/10.1038/nmeth.1318

430   Gu, P., Fang Gao, J., D'Souza, C. a, Kowalczyk, A., Chou, K.-Y., Zhang, L., 2012.

431   Trogocytosis of CD80 and CD86 by induced regulatory T cells. Cell. Mol. Immunol. 9,

432   136–146. https://doi.org/10.1038/cmi.2011.62

433   Hansen, J.D., Pasquier, L. Du, Lefranc, M.P., Lopez, V., Benmansour, A., Boudinot, P.,

434   2009. The B7 family of immunoregulatory receptors: A comparative and evolutionary

435   perspective. Mol. Immunol. 46, 457–472. https://doi.org/10.1016/j.molimm.2008.10.007

436   Hartley, G., Faulhaber, E., Caldwell, A., Coy, J., Kurihara, J., Guth, A., Regan, D., Dow, S.,

437   2016. Immune regulation of canine tumour and macrophage PD-L1 expression. Vet.

438   Comp. Oncol. n/a-n/a. https://doi.org/10.1111/vco.12197

439   Hwang, I., Huang, J.F., Kishimoto, H., Brunmark, A., Peterson, P.A., Jackson, M.R., Surh,

440   C.D., Zeling, C., Sprent, J., 2000. T cells can use either T cell receptor or CD28

441   receptors to absorb and internalize cell surface molecules derived from antigen-

442   presenting cells. J. Exp. Med. 191, 1137–1148. https://doi.org/10.1084/jem.191.7.1137

443   Ikebuchi, R., Konnai, S., Okagawa, T., Yokoyama, K., Nakajima, C., Suzuki, Y., Murata, S.,

444   Ohashi, K., 2014. Influence of PD-L1 cross-linking on cell death in PD-L1-expressing

445   cell lines and bovine lymphocytes. Immunology 142, 551–561.

446   https://doi.org/10.1111/imm.12243

447   Ikebuchi, R., Konnai, S., Okagawa, T., Yokoyama, K., Nakajima, C., Suzuki, Y., Murata, S.,

448   Ohashi, K., 2013. Blockade of bovine PD-1 increases T cell function and inhibits bovine

449   leukemia virus expression in B cells in vitro. Vet. Res. 44, 1–14.

450   https://doi.org/10.1186/1297-9716-44-59

451   Ikebuchi, R., Konnai, S., Shirai, T., Sunden, Y., Murata, S., Onuma, M., Ohashi, K., 2011.

452   Increase of cells expressing PD-L1 in bovine leukemia virus infection and enhancement

453   of anti-viral immune responses in vitro via PD-L1 blockade. Vet. Res. 42, 103–117.

454   https://doi.org/10.1186/1297-9716-42-103

455   Joly, E., Hudrisier, D., 2003. What is trogocytosis and what is its purpose? Nat. Immunol. 4,

456   815. https://doi.org/10.1038/ni0903-815

457   Kowarz, E., Löscher, D., Marschalek, R., 2015. Optimized Sleeping Beauty transposons

458   rapidly generate stable transgenic cell lines. Biotechnol. J. 10, 647–653.

459   https://doi.org/10.1002/biot.201400821

460   Lazenby, B.T., Tobler, M.W., Brown, W.E., Hawkins, C.E., Hocking, G.J., Hume, F.,

461   Huxtable, S., Iles, P., Jones, M.E., Lawrence, C., Thalmann, S., Wise, P., Williams, H.,

462   Fox, S., Pemberton, D., 2018. Density trends and demographic signals uncover the long-

463   term impact of transmissible cancer in Tasmanian devils. J. Appl. Ecol. 55, 1368–1379.

464   https://doi.org/10.1111/1365-2664.13088

465   Lemaoult, J., Caumartin, J., Daouya, M., Switala, M., Rebmann, V., Arnulf, B., Carosella,

466   E.D., 2015. Trogocytic intercellular membrane exchanges among hematological tumors.

467   J. Hematol. Oncol. 8, 25–27. https://doi.org/10.1186/s13045-015-0114-8

468   Luo, Z.X., Yuan, C.X., Meng, Q.J., Ji, Q., 2011. A Jurassic eutherian mammal and

469   divergence of marsupials and placentals. Nature 476, 442–445.

470   https://doi.org/10.1038/nature10291

471   Maekawa, N., Konnai, S., Ikebuchi, R., Okagawa, T., Adachi, M., Takagi, S., Kagawa, Y.,

472   Nakajima, C., Suzuki, Y., Murata, S., Ohashi, K., 2014. Expression of PD-L1 on canine

473   tumor cells and enhancement of IFN-g production from tumor-infiltrating cells by PD-

474   L1 blockade. PLoS One 9, e98415. https://doi.org/10.1371/journal.pone.0098415

475   Maekawa, N., Konnai, S., Okagawa, T., Nishimori, A., Ikebuchi, R., Izumi, Y., Takagi, S.,

476   Kagawa, Y., Nakajima, C., Suzuki, Y., Kato, Y., Murata, S., Ohashi, K., 2016.

477   Immunohistochemical analysis of PD-L1 expression in canine malignant cancers and

478   PD-1 expression on lymphocytes in canine oral melanoma. PLoS One 11, e0157176.

479   https://doi.org/10.1371/journal.pone.0157176

480   Maekawa, N., Konnai, S., Takagi, S., Kagawa, Y., Okagawa, T., Nishimori, A., Ikebuchi, R.,

481   Izumi, Y., Deguchi, T., Nakajima, C., Kato, Y., Yamamoto, K., Uemura, H., Suzuki, Y.,

482   Murata, S., Ohashi, K., 2017. A canine chimeric monoclonal antibody targeting PD-L1

483   and its clinical efficacy in canine oral malignant melanoma or undifferentiated sarcoma.

484   Sci. Rep. 7, 8951. https://doi.org/10.1038/s41598-017-09444-2

485   Mátés, L., Chuah, M.K.L., Belay, E., Jerchow, B., Manoj, N., Acosta-Sanchez, A., Grzela,

486   D.P., Schmitt, A., Becker, K., Matrai, J., Ma, L., Samara-Kuko, E., Gysemans, C.,

487   Pryputniewicz, D., Miskey, C., Fletcher, B., VandenDriessche, T., Ivics, Z., Izsvák, Z.,

488   2009. Molecular evolution of a novel hyperactive Sleeping Beauty transposase enables

489   robust stable gene transfer in vertebrates. Nat. Genet. 41, 753–761.

490   https://doi.org/10.1038/ng.343

491   Morton, P. a, Fu, X.T., Stewart, J. a, Giacoletto, K.S., White, S.L., Leysath, C.E., Evans, R.J.,

492   Shieh, J.J., Karr, R.W., 1996. Differential effects of CTLA-4 substitutions on the

493   binding of human CD80 (B7-1) and CD86 (B7-2). J. Immunol. 156, 1047–1054.

494   Murchison, E.P., Tovar, C., Hsu, A., Bender, H.S., Kheradpour, P., Rebbeck, C.A., Obendorf,

495   D., Conlan, C., Bahlo, M., Blizzard, C.A., Pyecroft, S., Kreiss, A., Kellis, M., Stark, A.,

496   Harkins, T.T., Marshall Graves, J.A., Woods, G.M., Hannon, G.J., Papenfuss, A.T.,

497   2010. The Tasmanian devil transcriptome reveals Schwann cell origins of a clonally

498   transmissible cancer. Science. 327, 84–87. https://doi.org/10.1126/science.1180616

499   Nakayama, M., Takeda, K., Kawano, M., Takai, T., Ishii, N., Ogasawara, K., 2011. Natural

500   killer (NK)-dendritic cell interactions generate MHC class II-dressed NK cells that

501   regulate CD4 + T cells. Proc. Natl. Acad. Sci. U. S. A. 108, 18360–18365.

502   https://doi.org/10.1073/pnas.1110584108

503   Nemoto, Y., Shosu, K., Okuda, M., Noguchi, S., Mizuno, T., 2018. Development and

504   characterization of monoclonal antibodies against canine PD-1 and PD-L1. Vet.

505   Immunol. Immunopathol. 198, 19–25. https://doi.org/10.1016/j.vetimm.2018.02.007

506   Patchett, A.L., Flies, A.S., Lyons, A.B., Woods, G.M., 2020. Curse of the devil: molecular

507   insights into the emergence of transmissible cancers in the Tasmanian devil (Sarcophilus

508   harrisii). Cell. Mol. Life Sci. https://doi.org/10.1007/s00018-019-03435-4

509   Pearse, A.-M., Swift, K., 2006. Allograft theory: transmission of devil facial-tumour disease.

510   Nature 439, 549. https://doi.org/10.1038/439549a

511   Pye, R.J., Pemberton, D., Tovar, C., Tubio, J.M.C., Dun, K.A., Fox, S., Darby, J., Hayes, D.,

512   Knowles, G.W., Kreiss, A., Siddle, H.V.T., Swift, K., Lyons, A.B., Murchison, E.P.,

513   Woods, G.M., 2016. A second transmissible cancer in Tasmanian devils. Proc. Natl.

514   Acad. Sci. U. S. A. 113, 374–379. https://doi.org/10.1073/pnas.1519691113

515   Qureshi, O.S., Zheng, Y., Nakamura, K., Attridge, K., Manzotti, C., Schmidt, E.M., Baker, J.,

516   Jeffery, L.E., Kaur, S., Briggs, Z., Hou, T.Z., Futter, C.E., Anderson, G., Walker,

517   L.S.K., Sansom, D.M., 2011. Trans-endocytosis of CD80 and CD86: A molecular basis

518   for the cell-extrinsic function of CTLA-4. Science. 332, 600–603.

519   https://doi.org/10.1126/science.1202947

520   Rebech, G.T., Venturin, G.L., Siqueira Ito, L.T., Bragato, J.P., De Carvalho Fonseca, B.S.,

521   Melo, L.M., Costa, S.F., De Rezende Eugênio, F., Dos Santos, P.S.P., De Lima, V.M.F.,

522   2020. PD-1 regulates leishmanicidal activity and IL-17 in dogs with leishmaniasis. Vet.

523   Immunol. Immunopathol. 219, 109970. https://doi.org/10.1016/j.vetimm.2019.109970

524   Robles, A., Qureshi, S.E., Stephen, S.J., Wilson, S.R., Burden, C.J., Taylor, J.M., Robles,

525   J.A., Qureshi, S.E., Stephen, S.J., Wilson, S.R., Burden, C.J., Taylor, J.M., 2012.

526   Efficient experimental design and analysis strategies for the detection of differential

527   expression using RNA-Sequencing. BMC Genomics 13, 484.

528   https://doi.org/10.1186/1471-2164-13-484

529   Siddle, H. V., Kreiss, A., Tovar, C., Yuen, C.K., Cheng, Y., Belov, K., Swift, K., Pearse, A.-

530   M.A.-M., Hamede, R., Jones, M.E., Skjødt, K., Woods, G.M., Kaufman, J., Skjodt, K.,

531   Woods, G.M., Kaufman, J., 2013. Reversible epigenetic down-regulation of MHC

532   molecules by devil facial tumour disease illustrates immune escape by a contagious

533   cancer. Proc. Natl. Acad. Sci. 110, 5103–8. https://doi.org/10.1073/pnas.1219920110

534   Tagawa, M., Maekawa, N., Konnai, S., Takagi, S., 2016. Evaluation of costimulatory

535   molecules in peripheral blood lymphocytes of canine patients with histiocytic sarcoma.

536   PLoS One 11, e0150030. https://doi.org/10.1371/journal.pone.0150030

537   Team, R.C., 2019. R: a language and for statistical computing.

538   U.S. Food and Drug Administration, 2020. KEYTRUDA® (pembrolizumab) injection, for

539   intravenous use Initial U.S. Approval: 2014.

540   U.S. Food and Drug Administration, 2011. YERVOY (ipilimumab) injection, for intravenous

541   use Initial U.S. Approval: 2011. U.S. Food Drug Adm. 1–32.

542

543

544